Light trapping in ultrathin CIGS solar cells with nanostructured back mirrors

Julie Goffard, Clément Colin, Fabien Mollica, Andrea Cattoni, Christophe Sauvan, Philippe Lalanne, Jean-François Guillemoles, Negar Naghavi and Stéphane Collin

***Abstract*—Novel architectures for light trapping in ultrathin Cu(In,Ga)Se_2 (CIGS) solar cells are proposed and numerically investigated. They are composed of a flat CIGS layer with nanostructured back mirrors made of highly reflective metals. Multi-resonant absorption is obtained for two different patterns of nanostructured mirrors. It leads to a dramatic increase in the short-circuit current predicted for solar cells with very thin CIGS layers. We analyse the resonance phenomena and the density of photogenerated carriers in the absorber. We discuss the impact of the material used for the buffer layer (CdS, ZnS) and the back mirror (Mo, Cu, Au, Ag). We investigate various CIGS thicknesses from 100 nm to 500 nm, and we compare our numerical results with experimental data taken from the literature. We predict a short-circuit current of Jsc = 33.6 mA/cm^2 for a realistic solar cell made of 200 nm-thick CIGS absorber with a copper nanostructured mirror. It opens a way toward ultrathin CIGS solar cells with potential conversion efficiencies up to 20%.**

***Index Terms*—Photovoltaic cells, Absorption, CIGS and CdTe Thin Film Solar Cells, Nanostructures, Modeling, Nanophotonics**

I. Introduction

THE Cu(In,Ga)Se_2 (CIGS) solar cell technology has recorded continuous performance improvements over the past few years with conversion efficiencies up to 22.6% [1], [2]. Record CIGS solar cells are obtained with 2-3 μm-thick films and CdS or ZnS buffer layers. However, material savings are required to overcome the bottleneck of the limited primary resources, and the thickness reduction of the CIGS absorber layer is a key for targeted multi-GW yearly production levels. It has been shown that high performance can be maintained for CIGS thicknesses down to 1 μm [3]–[8]. However, keeping the same architecture with thinner absorbers results in decline of both the open circuit voltage (Voc) and the short-circuit current (Jsc). The Voc drop is mainly due to back surface recombinations and can be avoided through efficient surface passivation using for instance rear point contacts through nanostructured dielectric layers [9]–[13]. Improved light trapping is required in order to keep high Jsc in ultrathin CIGS solar cells. The conventional Mo back contact induces parasitic absorption. It should be replaced by a material with a higher reflectivity and a good ohmic contact with CIGS. The use of alternative solutions such as ZrN, Au, MoO_x and transparent conducting oxide (TCO) have been investigated on planar cells [14]–[18]. At long wavelengths, further optical path enhancement is required. Lambertian back reflectors [19] or periodic textures [20] have been investigated numerically. Experiments with ZnO nanowires [21] and silica nanospheres [22] have demonstrated the potential of nanostructure arrays for enhanced light trapping in ultrathin (< 0.5 μm) solar cells. Most of these strategies make use of rough or textured CIGS layers and may have a negative impact on non-radiative surface recombinations.

Here, we propose a novel light trapping strategy based on a flat and ultrathin CIGS layer with a nanostructured back mirror. Periodical nanostructures enable coupling of incoming light into resonant modes in the structure [23]–[26]. Two complementary structures are proposed for the nanostructured back mirror. Their geometrical parameters are optimized in order to achieve a broadband multi-resonant absorption spectrum resulting in a high Jsc. The density profiles of photogenerated carriers of both structures are analyzed and compared, and the influence of the materials (buffer layer, metallic back mirror) and CIGS thickness are investigated.

II. Architecture of the solar cells

The structures studied in this work aimed at simulating a realistic CIGS solar cell with CIGS layer thicknesses (h_{CIGS}) between 100 nm and 500 nm, and a bandgap of 1.15eV. The stack is composed of conventional ZnO:Al/i-ZnO/CdS/CIGS layers with respective thicknesses 100nm/70nm/50nm/h_{CIGS}. In the frame of this paper, the CdS layer can be replaced by a ZnS layer of the same thickness. The conventional Mo back contact is replaced by a nanostructured mirror made of Ag, Au or Cu in order to improve light trapping in the CIGS layer. Two complementary geometries of the nanostructured metallic mirror are studied and compared. The two types of solar cells are depicted in Fig. 1a and b. Numerical calculations have been performed with a rigourous coupled wave analysis (RCWA) method [27]–[30]. We consider impinging plane waves at normal incidence, linearly polarized along the x axis, and we calculate absorption in each layer. The refractive indices used for each material are given in Appendix A. The

J. Goffard, A. Cattoni and S. Collin are with the Centre for Nanoscience and Nanotechnology, CNRS, Univ. Paris-Sud, Université Paris-Saclay, C2N - Marcoussis, 91460 Marcoussis, France

F. Mollica, Jean-François Guillemoles and N. Naghavi are with the Institute of Research & Development on Photovoltaic Energy (IRDEP), CNRS UMR 7174, 6 quai Watier, 78400 Chatou, France

C. Sauvan is with the Laboratoire Charles Fabry, Institut d'Optique Graduate School, CNRS, Université Paris-Saclay, 91127 Palaiseau, France

P. Lalanne is with the Laboratoire Photonique, Numérique et Nanosciences (LP2N), UMR 5298, CNRS - IOGS - Univ. Bordeaux, 33400 Talence, France

C. Colin is now with the Laboratoire Nanotechnologies Nanosystèmes (LN2) - CNRS UMI-3463, Institut Interdisciplinaire d'Innovation Technologique (3IT), Université de Sherbrooke, 3000 Boulevard Université, Sherbrook, J1K 0A5, Québec, Canada

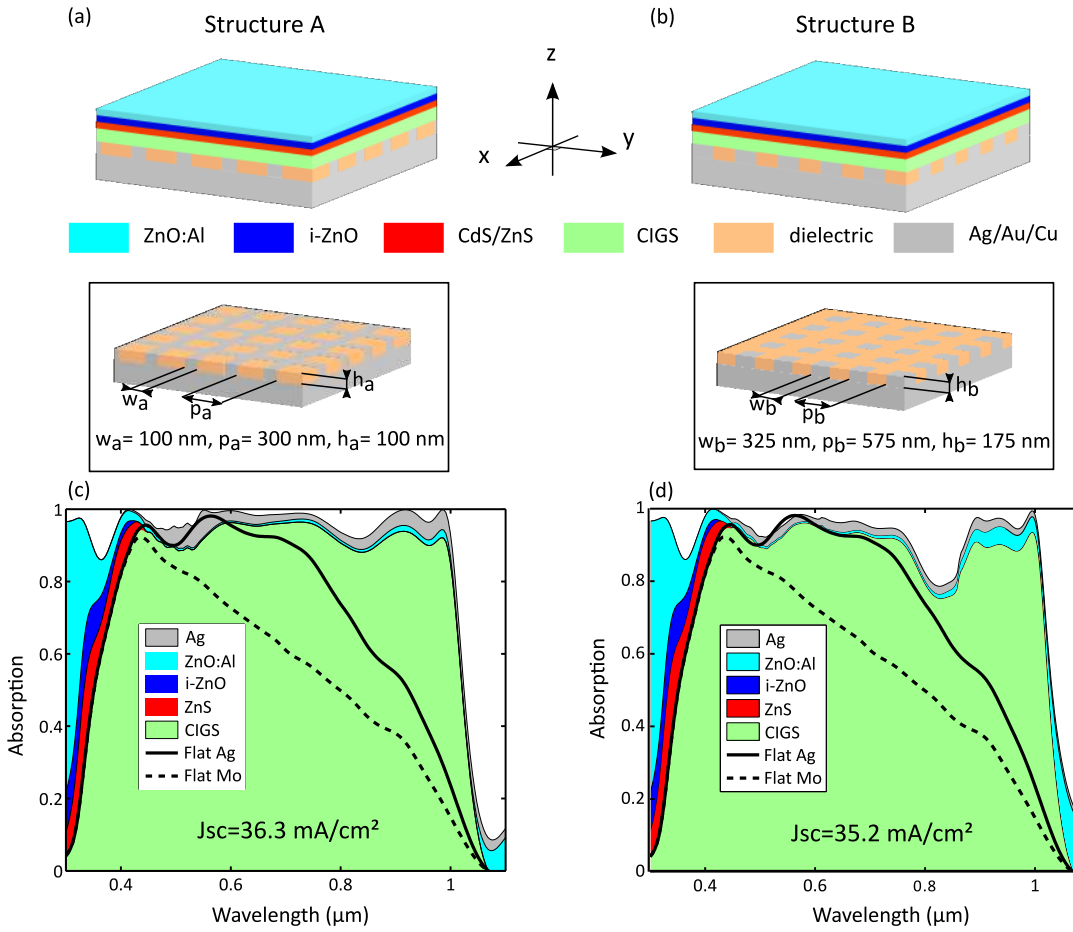

Figure 1. (a,b): Sketches of a CIGS solar cell with a nanostructured back mirror. The structure is composed of top ZnO:Al (light blue), i-ZnO (blue), ZnS or CdS (red), CIGS (green), and a nanostructured mirror (grey) embedded in a dielectric medium (brown). Inset: Sketch of the nanostructured mirror (structure A: Ag nanogrid ; structure B: Ag nanopillars). (c,d): Absorption spectra of structures A (c) and B (d) calculated for a 150 nm-thick CIGS solar cell with a silver nanostructured back mirror. Absorption in each layer of the stack is shown (color areas). Absorption in the CIGS layer (green) is compared to results obtained with a flat back contact made of Mo (dotted line) or Ag (continuous line).

dielectric material embedded between the CIGS layer and the nanostructured mirror is made of TiO_2 and modelled with a constant refractive index of 1.9. The numerical results obtained with planar layers of different thicknesses are consistent with external quantum efficiencies published in reference [10], see Appendix B.

In the two cases, the geometrical parameters have been optimized for a cell with a 150 nm-thick CIGS layer, a ZnS buffer layer and a Ag nanostructured mirror. Structure A is made of a 100 nm-thick square Ag grid (width: 100 nm, period: 300 nm). Structure B is made of 175 nm-thick square Ag pillars (width: 325 nm, period: 575 nm). The unit cells are composed of 56% of Ag in structure A, and 32% in structure B. This difference in the fill factor will change the influence of metallic parasitic absorption as it will be shown in the next section. These structures will be called the "optimized structures" in the rest of this paper. These geometrical parameters are fixed throughout the paper and the impact of other materials and CIGS thicknesses will be investigated.

III. Multi-resonant absorption

In this section, we first analyze the optical properties obtained for the optimized structures made of 150 nm-thick CIGS. Absorption in each layer of the stack is plotted in Fig. 1c and d (color areas). Very efficient absorption is achieved in the CIGS layer (green region). It can be compared to absorption obtained with the same structure composed of a flat Mo (dotted curve) or Ag back contact (solid curve). The theoretical short circuit current is calculated as follows:

$$J_{sc} = \frac{q}{hc}\int_{\lambda_i}^{\lambda_f} A(\lambda)P(\lambda)\lambda \mathrm{d}\lambda = \frac{q}{S}\int_V G(\mathbf{r})\mathbf{d^3r} \qquad (1)$$

where q, h, and c are respectively the electron charge, the Planck's constant, and the speed of light. S and V are the surface area and volume of the absorber, respectively. $A(\lambda)$ is the calculated absorption in the CIGS layer, $P(\lambda)$ is the incident spectral power density per unit area associated to the normalized AM1.5G solar spectrum, and $G(r)$ is the density of photogeneration rate (number of photogenerated carriers per unit volume and time). For CIGS solar cells, the Jsc is obtained by integration over the wavelength range [$\lambda_i = 300$ nm ; $\lambda_f =$

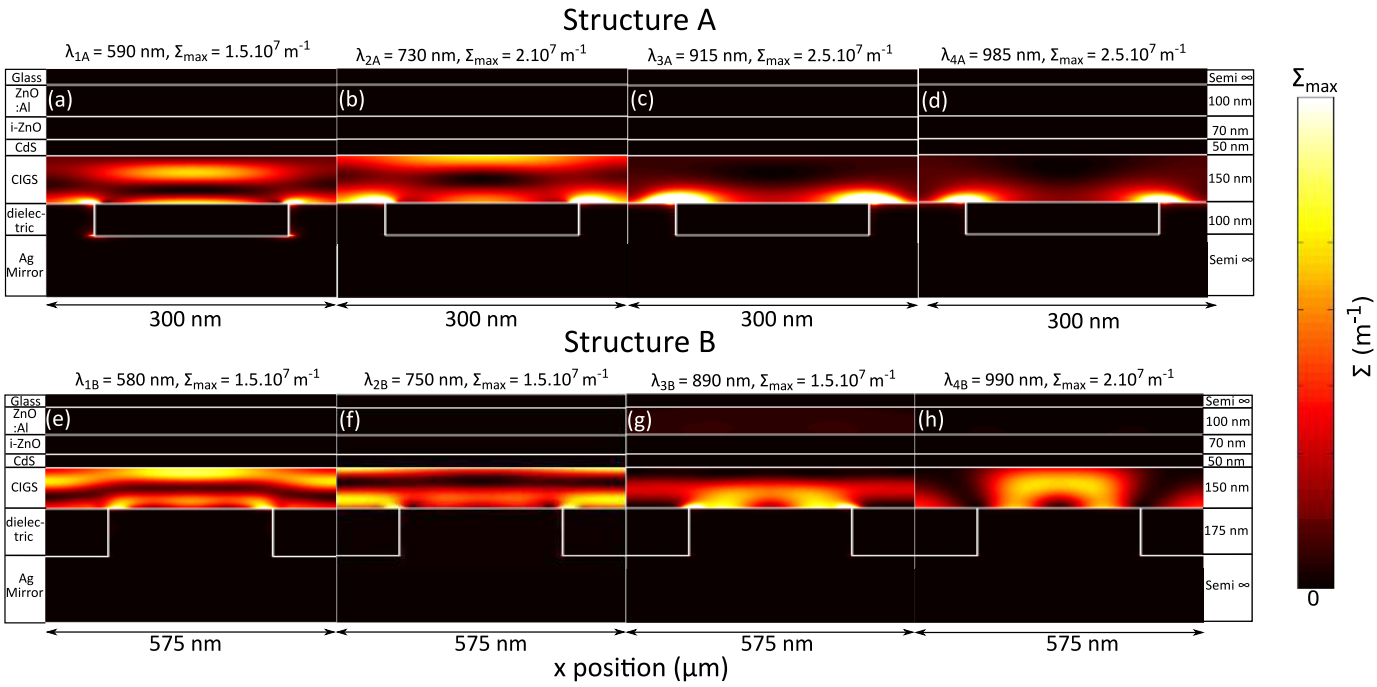

Figure 2. Maps of the density of absorbed photons in the optimized solar cells A and B of Fig. 1. Cross-sections of $\Sigma(\lambda, x, y, z)$ at resonance wavelengths for structure A (a) $\lambda_{1A} = 590$ nm, (b) $\lambda_{2A} = 730$ nm, (c) $\lambda_{3A} = 915$ nm, (d) $\lambda_{4A} = 985$ nm and structure B (e) $\lambda_{1B} = 580$ nm, (f) $\lambda_{2B} = 750$ nm, (g) $\lambda_{3B} = 890$ nm and (h) $\lambda_{4B} = 990$ nm. The maps are plotted at y=0 in the (x,z) plane, with a linearly polarized incident plane wave along x direction. The color scale represents $\Sigma(\lambda, x, y, z)$ on a linear scale from 0 to Σ_{max}, and Σ_{max} is given for each map.

1100 nm]. A perfect collection of photogenerated charges is assumed. The resulting Jsc is thus an upper limit value.

In case of flat Mo, low reflectivity and huge parasitic absorption in the back contact results in single-pass absorption and low short-circuit current ($Jsc = 23.5$ mA/cm^2). By replacing the Mo contact by a flat Ag mirror, parasitic absorption is avoided and light absorption is above 90 % for $\lambda < 700$ nm. At $\lambda = 700$ nm, absorption is improved by 30 % compared to Mo. Efficient light reflection on Ag leads to a double-pass absorption in the CIGS layer and almost 31 mA/cm^2 in short-circuit current density.

The nanostructured Ag mirror provides further light absorption improvement with additional peaks between $\lambda = 700$ nm and $\lambda = 1000$ nm in the two structures. Efficient absorption is achieved over the whole visible and near-infrared spectral domain, with a 91.6 % average CIGS absorption in the 400 nm-1000 nm wavelength range for structure A and 90% for structure B. It results in a Jsc of (A) 36.3 mA/cm^2 and (B) 35.2 mA/cm^2, respectively. These values are close to Jsc of record ∼2.5 µm CIGS cells [1], [2], and corresponds to an increase of > 50 % over solar cells with flat Mo back contact.

In Fig. 1c and d, the red, dark blue, light blue and grey curves show absorption in the ZnS, i-ZnO, ZnO:Al and silver layers, respectively. Overall parasitic absorption is very low, except in the ZnO:Al layer below $\lambda = 400$ nm. Parasitic absorption in the nanostructured Ag back mirror accounts for less than 2% for both structures.

IV. Origin of the resonant peaks

For both structures A and B, the strong absorption improvement between λ = 600 nm and λ = 1050 nm in Fig. 1 (c,d) originates from multi-resonant absorption. We identify four main peaks: $\lambda_{1A} = 590$ nm, $\lambda_{2A} = 730$ nm, $\lambda_{3A} = 915$ nm and $\lambda_{4A} = 985$ nm for structure A, and $\lambda_{1B} = 580$ nm, $\lambda_{2B} = 750$ nm, $\lambda_{3B} = 890$ nm and $\lambda_{4B} = 990$ nm for structure B.

In the following, we use the electric field intensity at position (x,y,z) in order to analyze each resonance mechanism. In Fig. 2, we have plotted of $\Sigma = \rho/\Phi_{in}$, where ρ is the density of absorbed photons (per unit time) and Φ_{in} is the incident photon flux. These quantities can be expressed as:

$$\Sigma(\lambda, x, y, z) = \frac{2\pi\Im(\epsilon_r)}{\lambda}\left|\frac{E(\lambda, x, y, z)}{E_0}\right|^2, \quad (2)$$

$$\rho(\lambda, x, y, z) = \frac{\epsilon_0\Im(\epsilon_r)}{2\hbar}|E(\lambda, x, y, z)|^2, \quad (3)$$

$$\Phi_{in}(\lambda) = \frac{\epsilon_0\lambda}{2h}|E_0|^2, \quad (4)$$

where ϵ_0 is the dielectric permittivity of vacuum, $\Im(\epsilon)$ is the position-dependent imaginary part of the relative dielectric permittivity, and E_0 and $E(\lambda, x, y, z)$ are the electric field amplitude of the incident plane wave and in the structure, respectively. Fig. 2 shows the cross-sections of $\Sigma(\lambda, x, y, z)$ in the (x, z) plane at $y = 0$ for each resonance.

At short wavelengths ($\lambda < 800$ nm), the electric field features stationary waves along the z axis for both structures. At these wavelengths, the field is nearly constant along the (x, y) axis, see Fig. 2 (a,b,e,f). Similar Fabry-Perot resonances are found with a flat silver mirror at a slightly smaller wavelengths ($\lambda = 560$ nm and $\lambda = 700$ nm, see Fig. 1). The pattern of the back mirror has a small impact, but provides slightly improved absorption in this wavelength range.

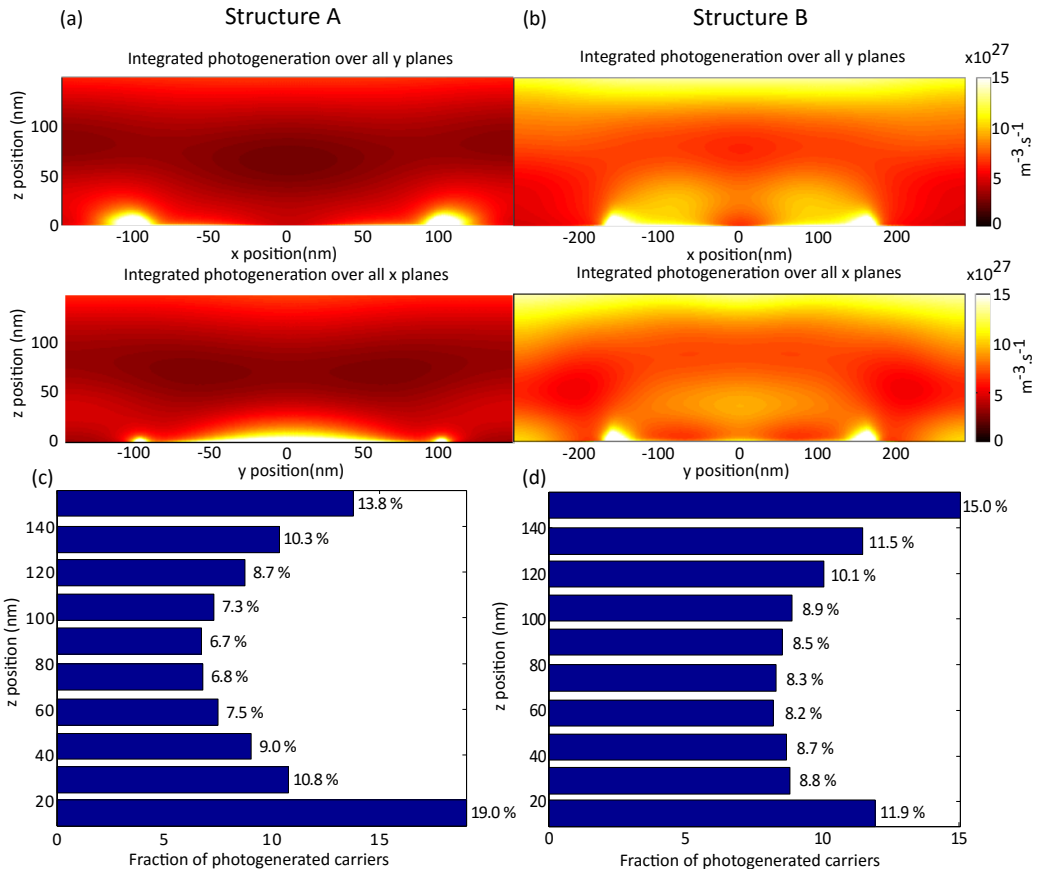

Figure 3. Density of photogenerated carriers in the CIGS layer calculated for the optimized solar cells A and B of Fig. 1 (ZnO:Al/i-ZnO/CdS/CIGS/nanostructured Ag layers with respective thicknesses 100nm/70nm/50nm/150nm/$h_A$or h_B, $h_A = 100$ nm and $h_B = 175$ nm). Maps of photogenerated carriers integrated over y and x are presented for structures A (a) and B (b). z-profiles of the photogenerated carriers integrated by slices of 15 nm in the z direction are presented for structures A (c) and B (d).

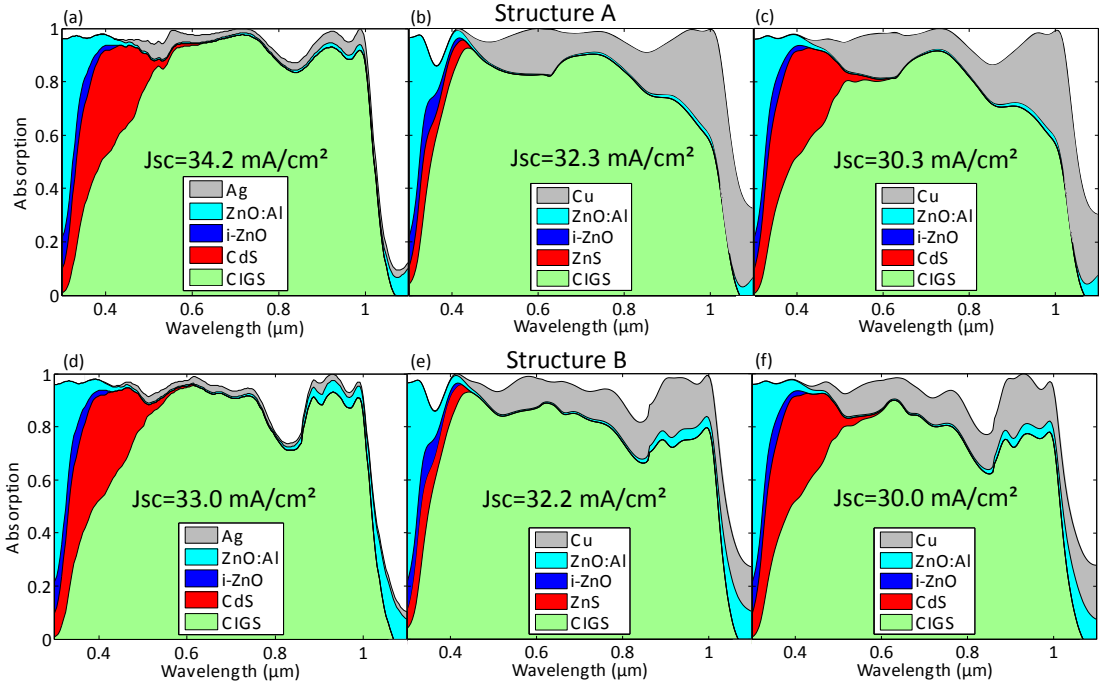

Figure 4. Absorption spectra calculated for solar cells A (a,b,c) and B (d,e,f) with a CIGS thickness of 150 nm and stacks of layers similar to Fig. 1, with the following changes: (a,d) CdS buffer layer and Ag nanostructured mirror ; (b,e) ZnS buffer layer and Cu nanostructured mirror ; (c,f) CdS buffer layer and Cu nanostructured mirror.

Above $\lambda = 800$ nm, nanostructured mirrors have a strong impact and result in absorption enhancements by a factor of two as compared to the flat mirror. They are responsible for diffraction effects in the absorber layer, resulting in strong variations of the electric field along the x and y axis.

In the case of structure A, most of the absorption is localized close to the back surface of the CIGS layer, in the vicinity of the metal nanogrid (Fig. 2 (c,d)). It leads to significant absorption improvement despite the low CIGS absorptivity in this spectral region. For instance at λ_{4A}, absorption is increased from 30 % for double-pass absorption (flat Ag) to 92 % with the nanostructured Ag mirror.

Structure B features higher absorption in the middle of the CIGS layer, with absorption maxima above the metal nanopillars. At λ_{4B}, absorption is increased from 26 % for double-pass absorption (flat Ag) to 93% with the nanostructured Ag mirror.

V. Spatial dependence of the photogenerated carrier density

The spatial dependence of the carriers photogenerated in the CIGS layer is analyzed in Fig. 3a and b. The photogenerated carriers rate can be simply expressed with $\Sigma(\lambda, x, y, z)$ and the incident spectral power density $P(\lambda)$:

$$G(x, y, z) = \int_{\lambda_i}^{\lambda_f} \Sigma(\lambda, x, y, z) P(\lambda) \mathrm{d}\lambda. \quad (5)$$

The density of photogenerated carriers is first integrated along x and y directions for structure A (Fig. 3(a)) and structure B (Fig. 3(b)). In both cases, the photogenerated carrier density is almost constant in the (x, y) plane near the top ZnS/CIGS interface while the nanostructured mirror induces inhomogeneities at the bottom interface. In structure A, many carriers are generated in the vicinity of the nanostructured mirror, with a strong localization at the dielectric/CIGS interface and close to the silver nanogrid edges. In structure B, the maximum density of photogenerated carriers is localized close to the silver nanopillars of the back mirror. The lower contrast of cross-section maps (b) reveal a more homogeneous density of photogenerated carriers in the CIGS layer of structure B.

The difference between the two structures is also highlighted in Fig. 3(c) and (d) which present the z-profile of the photogenerated carrier density. The CIGS layer is decomposed into 15 nm-thick slices. In both structures, about one third of the total carriers are generated close to the interfaces, in the top and bottom 15 nm-thick regions. However, much more carriers are generated close to the bottom interface in structure A as compared to structure B (19 % versus 11.9 %). This architecture would require efficient passivation layers in order to avoid surface recombinations [9], [12]. Structure B features a more homogeneous density of photogenerated carriers in the CIGS volume, and should be more favorable for efficient carrier transport and collection.

VI. Influence of the buffer layer and back mirror

In the previous calculations, the materials have been chosen in order to minimize parasitic absorption in the stacked layers and optimize absorption in the CIGS layer. The use of some of these materials is unusual and may be questionable for a real device application. ZnS is used as a buffer layer in order to minimize short-wavelength absorption, but CdS is still widely used in CIGS solar cells and led to record efficiencies [1]. The choice of silver for the nanostructured back mirror is motivated by its high reflectivity in the visible and near infrared range. However, it may be unsuitable for high performance solar cells due to silver diffusion in CIGS and the quality of the CIGS/Ag ohmic contact. In the following, we investigate the impact of these materials and replace ZnS by CdS and Ag by Cu or Au.

A. CdS versus ZnS

Figs. 4(a,d) show absorption spectra for a device with a nanostructured Ag mirror and a CdS buffer layer for the two structures (A,B). The green area corresponds to CIGS absorption. The parasitic CdS absorption in the 300-500 nm range is highlighted in red. At $\lambda = 400$ nm, CIGS absorption decreases from 90% with ZnS to 55% with CdS. The short-circuit current drops accordingly from 36.3 mA/cm^2 to 34.2 mA/cm^2 (structure A) and from 35.2 mA/cm^2 to 33 mA/cm^2 (structure B). The two structures present similar results since the geometry of the mirror as no influence on this parasitic absorption.

B. Cu or Au versus Ag

Our studies have shown that Au and Cu mirrors give almost the same optical response. We have found slightly less absorption in gold (see Appendix C), but copper is a cheaper and a more viable solution. Figs. 4(b,e) show the results obtained with a nanostructured Cu mirror and ZnS buffer layer with the same grating parameters than the optimized structures. In structure A (Fig. 4(b)), the effect of multiresonant absorption is smoothed (resonant peaks disappear in the CIGS layer) by the parasitic absorption in the Cu (grey area). On the contrary, resonant peaks are still present in the CIGS absorption spectrum of structure B in the 800 nm-1000 nm spectral range, with less parasitic absorption. This is consistent with the lower density of photogenerated carriers at the bottom interface than in A. It results in almost the same Jsc ($\sim$32 mA/cm^2) for the two structures.

C. CdS buffer layer and Cu nanostructured mirror

Figs. 4(c,f) show the results obtained with the combination of a CdS buffer layer and a Cu nanostructured mirror. In this case, parasitic absorption at short and long wavelengths results in a Jsc decrease down to 30.3 mA/cm^2 for structure A and 30.0 mA/cm^2 for structure B. In spite of the accumulation of parasitic absorptions, the Jsc stays above 30 mA/cm^2 for only 150 nm-thick of CIGS for both structures, and is still 29 % higher than the same stack with a flat Mo back contact.

VII. Influence of the CIGS layer thickness

We have also studied the influence of the CIGS thickness on the short-circuit current for each material used in the back mirror. The full set of results is given in appendix

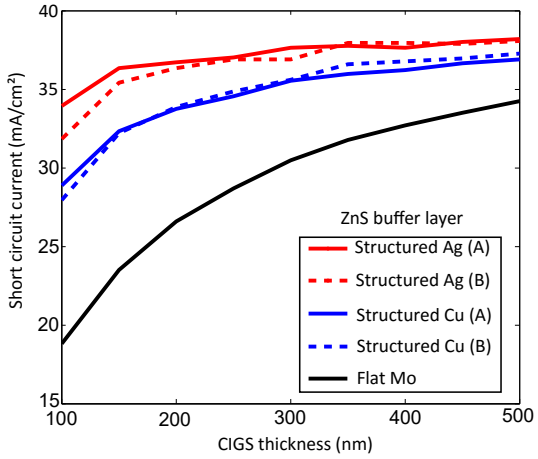

Figure 5. Short-circuit current density (Jsc) as a function of the CIGS thickness for solar cells with a stack of layers similar to Fig. 1 (ZnS buffer layer), and three different back mirrors: a flat Mo back contact (dark curve), and nanogrid (structure A, continuous curves) or nanopillar (structure B, dashed curves) back mirrors made of Ag (red curves) or Cu (blue curves).

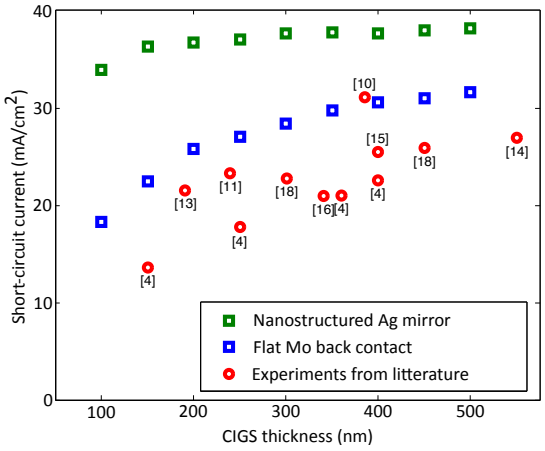

Figure 6. Comparison between numerical calculations and experimental results taken from the literature. Short-circuit current density (Jsc) as a function of the CIGS thickness. Square markers corresponds to numerical results for solar cells composed of conventional ZnO:Al/i-ZnO/CdS/CIGS stack layers with respective thicknesses 100nm/70nm/50nm/h_{CIGS} and a Mo back contact (blue markers) or a nanostructured Ag grid (green markers). Red circles corresponds to Jsc published in the literature with ultrathin CIGS solar cells composed of similar stack layers with Mo back contacts [4], [10], [11], [13], or alternative back reflectors [14]–[16], [18]. Note that B. Vermang *et al.* and E. Jarzembowski *et al.* have inserted thin nanostructured passivation layers between the CIGS layer and Mo back contact [10], [11], [13].

C. Fig. 5 shows the evolution of Jsc as a function of the CIGS thickness from 100 nm to 500 nm, for a flat Mo back contact (black curve), a Cu nanogrid mirror (blue curve), a Cu nanopillar mirror (blue dashed curve), a Ag nanogrid mirror (red curve) and a Ag nanopillar mirror (red dashed curve). The geometrical parameters of the nanostructured back mirror are kept constant and correspond to the structure optimized for a thickness of 150 nm with a silver mirror (structure A: width = 200 nm, period = 300 nm and height = 100 nm, structure B: width = 325 nm, period = 575 nm and height = 175 nm), as presented in section II. The Ag nanogrid mirror (structure A) with a ZnS buffer layer shows the best performances for the whole thickness range. As expected, the impact of the nanostructured mirror increases for thinner absorbers. For 100 nm-thick CIGS layers, Jsc is enhanced by 80 % with Ag nanogrid as compared to the flat Mo contact. The Cu nanopillar mirror (structure B) appears as a good compromise with high Jsc, no cost issue and nearly the same work function than Mo [15]. A promising Jsc = 34 mA/cm^2 is predicted for a 200 nm-thick CIGS layer with a Cu nanopillar mirror and a ZnS buffer layer. This is a 28% enhancement as compared to the same structure with a Mo flat mirror (Jsc = 26.5 mA/cm^2).

VIII. Comparison with experiments

We have compared our numerical results with experiments found in the literature for CIGS thickness between 100 nm and 550 nm and bandgap around 1.15 eV. In figure 6, we report the results of our numerical calculations for a conventional stack of layers ZnO:Al/i-ZnO/CdS/CIGS with respective thicknesses 100nm/70nm/50nm/h_{CIGS}, and a Mo back contact (blue markers) or a nanostructured Ag grid (green markers). Red circles show Jsc taken from the literature, for ultrathin CIGS solar cells composed of similar stack layers with respective thicknesses 300-400 nm/50-100 nm/40-50 nm/h_{CIGS}. A Mo back contact is used in reference [4] with four different thicknesses. The thickness dependence of Jsc has a similar trend for numerical and experimental results. The much lower Jsc measured by Lundberg *et al.* is attributed to reduced carrier collection efficiency which originates from increased recombinations at the back contact. Much higher collection efficiency has been obtained by adding thin passivation layers with nano-sized point contacts between the CIGS and Mo layers [10], [11], [13], resulting in Jsc close to our numerical calculations. Jsc can also be increased by introducing alternative back contacts with higher reflectivity, as shown in references [14]–[16], [18]. It is worth mentioning that the difference between numerical and experimental results can also originate from additional optical losses in both window and buffer layers (free-carrier absorption, increased thicknesses,...).

IX. Conclusion

The optical properties of ultra-thin CIGS solar cells with two geometries of nanostructured back mirrors were numerically studied with a RCWA based optical simulation program. A very high short-circuit current (Jsc = 36.3 mA/cm^2) is obtained for 150 nm-thick CIGS with an optimized nanogrid Ag mirror (width: 200 nm and period: 300 nm) and a ZnS buffer layer. This high short-circuit current originates from multi-resonant absorption with several peaks in the 600-1000 nm spectral range. They are studied with electromagnetic field intensity maps and result in inhomogeneous photogenerated carriers in the absorber. We have highlighted a higher density of carriers generated close to the upper and lower CIGS interfaces for nanostructured mirror. This feature suggests that the performances expected with these architectures should be very sensitive to surface passivation. This effect could be studied by full opto-electrical simulation based on the exact three-dimensional profile of the density of photogenerated

carriers in the absorber volume. We have also investigated the impact of the material used as buffer layers (CdS, ZnS) and back mirrors (Mo, Cu, Au, Ag), and we have demonstrated that a nanopillar geometry with Cu limits the impact of the parasitic absorption in the nanostructrured mirror. It is worth noting that Cu and Ag mirrors on CIGS may be unstable and lead to copper selenide or silver selenide phases, respectively. This issue may be circumvented by adding a very thin TCO layer between the CIGS and the nanostructured back mirror. Thicknesses of only a few nanometers should be sufficient to prevent diffusion of metals with a negligible impact on the optical response of the solar cell. We have also compared our numerical calculations with experimental data taken from the literature. Similar trends are observed for the thickness dependence of the short-circuit current. This comparison emphasizes the importance of low surface recombination and low parasitic losses in order to reach Jsc values predicted by numerical calculations. Assuming state-of-the-art electrical performances (Voc=750 mV, FF=79.4% [1]), a conversion efficiency of 20% requires a short-circuit current Jsc=33.6 mA/cm^2. This 20 %-efficiency target could be reached with a realistic architecture made of only 200 nm-thick CIGS layers, a ZnS buffer layer and a nanopillar Cu mirror.

REFERENCES

[1] T. Friedlmeier, P. Jackson, A. Bauer, D. Hariskos, O. Kiowski, R. Wuerz, and M. Powalla, "Improved photocurrent in Cu(In,Ga)Se_2 solar cells: From 20.8% to 21.7% efficiency with CdS buffer and 21.0% Cd-free," *IEEE Journal of Photovoltaics*, vol. 5, no. 5, pp. 1487–1491, 2015.

[2] P. Jackson, R. Wuerz, D. Hariskos, E. Lotter, W. Witte, and M. Powalla, "Effects of heavy alkali elements in Cu(In,Ga)Se_2 solar cells with efficiencies up to 22.6%," *physica status solidi (RRL) - Rapid Research Letters*, vol. 10, no. 8, pp. 583–586, 2016. [Online]. Available: http://dx.doi.org/10.1002/pssr.201600199

[3] T. Negami, S. Nishiwaki, Y. Hashimoto, and N. Kohara, "Effect of absorber thickness on performance of Cu(In,Ga)Se_2 solar cells," in *2nd World Conference and Exhibition on Photovoltaic Solar Energy Conversion*, 1998, pp. 1181–1184.

[4] O. Lundberg, M. Bodegård, J. Malmström, and L. Stolt, "Influence of the Cu(In,Ga)Se_2 thickness and Ga grading on solar cell performance," *Progress in Photovoltaics: Research and Applications*, vol. 11, no. 2, pp. 77–88, 2003.

[5] K. Ramanathan, R. Noufi, B. To, D. l. Young, R. Bhattacharya, M. A. Contreras, R. G. Dhere, and G. Teeter, "Processing and properties of sub-micron CIGS solar cells," in *2006 IEEE 4th World Conference on Photovoltaic Energy Conference*, vol. 1, 2006, pp. 380–383.

[6] M. Gloeckler and J. R. Sites, "Potential of submicrometer thickness Cu(In,Ga)Se_2 solar cells," *Journal of Applied Physics*, vol. 98, no. 10, p. 103703, 2005.

[7] Z. Jehl, F. Erfurth, N. Naghavi, L. Lombez, I. Gerard, M. Bouttemy, P. Tran-Van, A. Etcheberry, G. Voorwinden, B. Dimmler, W. Wischmann, M. Powalla, J. F. Guillemoles, and D. Lincot, "Thinning of CIGS solar cells: Part II: Cell characterizations," *Thin Solid Films*, vol. 519, no. 21, pp. 7212–7215, 2011.

[8] N. Amin, P. Chelvanathan, M. I. Hossain, and K. Sopian, "Numerical modelling of ultra thin Cu(In,Ga)Se_2 solar cells," *Energy Procedia*, vol. 15, pp. 291–298, 2012.

[9] B. Vermang, V. Fjällström, J. Pettersson, P. Salomé, and M. Edoff, "Development of rear surface passivated Cu(In,Ga)Se_2 thin film solar cells with nano-sized local rear point contacts," *Solar Energy Materials and Solar Cells*, vol. 117, pp. 505–511, 2013.

[10] B. Vermang, J. T. Wätjen, V. Fjällström, F. Rostvall, M. Edoff, R. Kotipalli, F. Henry, and D. Flandre, "Employing Si solar cell technology to increase efficiency of ultra-thin Cu(In,Ga)Se_2 solar cells," *Prog. Photovolt: Res. Appl.*, vol. 22, no. 10, pp. 1023–1029, 2014.

[11] B. Vermang, J. T. Wätjen, C. Frisk, V. Fjällström, F. Rostvall, M. Edoff, P. Salomé, J. Borme, N. Nicoara, and S. Sadewasser, "Introduction of Si PERC rear contacting design to boost efficiency of Cu(In,Ga)Se_2 solar cells," *IEEE Journal of Photovoltaics*, vol. 4, no. 6, pp. 1644–1649, 2014.

[12] B. Vermang, V. Fjällström, Xindong Gao, and M. Edoff, "Improved rear surface passivation of Cu(In,Ga)Se_2 solar cells: a combination of an Al_2O_3 rear surface passivation layer and nanosized local rear point contacts," *IEEE Journal of Photovoltaics*, vol. 4, no. 1, pp. 486–492, 2014.

[13] E. Jarzembowski, B. Fuhrmann, H. Leipner, W. Fränzel, and R. Scheer, "Ultrathin Cu(In,Ga)Se_2 solar cells with point-like back contact in experiment and simulation," *Thin Solid Films*, 2016. [Online]. Available: http://www.sciencedirect.com/science/article/pii/S0040609016306885

[14] J. Malmström, S. Schleussner, and L. Stolt, "Enhanced back reflectance and quantum efficiency in Cu(In,Ga)Se_2 thin film solar cells with a ZrN back reflector," *Applied Physics Letters*, vol. 85, no. 13, pp. 2634–2636, 2004.

[15] Z. J. Li-Kao, N. Naghavi, F. Erfurth, J. F. Guillemoles, I. Gérard, A. Etcheberry, J. L. Pelouard, S. Collin, G. Voorwinden, and D. Lincot, "Towards ultrathin copper indium gallium diselenide solar cells: proof of concept study by chemical etching and gold back contact engineering," *Progress in Photovoltaics: Research and Applications*, vol. 20, no. 5, pp. 582–587, 2012.

[16] J. K. Larsen, H. Simchi, P. Xin, K. Kim, and W. N. Shafarman, "Backwall superstrate configuration for ultrathin Cu(In,Ga)Se_2 solar cells," *Applied Physics Letters*, vol. 104, no. 3, p. 033901, 2014.

[17] N. Dahan, Z. Jehl, T. Hildebrandt, J.-J. Greffet, J.-F. Guillemoles, D. Lincot, and N. Naghavi, "Optical approaches to improve the photocurrent generation in Cu(In,Ga)Se_2 solar cells with absorber thicknesses down to 0.5 μm," *Journal of Applied Physics*, vol. 112, no. 9, pp. 094 902–094 902–7, 2012.

[18] F. Mollica, M. Jubault, F. Donsanti, A. Loubat, M. Bouttemy, A. Etcheberry, and N. Naghavi, "Light absorption enhancement in ultra-thin Cu(In,Ga)Se_2 solar cells by substituting the back-contact with a transparent conducting oxide based reflector," *Thin Solid Films*, 2016. [Online]. Available: http://www.sciencedirect.com/science/article/pii/S0040609016305946

[19] N. Dahan, Z. Jehl, J. F. Guillemoles, D. Lincot, N. Naghavi, and J.-J. Greffet, "Using radiative transfer equation to model absorption by thin Cu(In,Ga)Se_2 solar cells with lambertian back reflector," *Optics Express*, vol. 21, no. 3, p. 2563, 2013.

[20] C. Onwudinanti, R. Vismara, O. Isabella, L. Grenet, F. Emieux, and M. Zeman, "Advanced light management based on periodic textures for Cu(In,Ga)Se_2 thin-film solar cells," *Optics Express*, vol. 24, no. 6, pp. A693–A707, 2016.

[21] W. Ohm, W. Riedel, U. Askunger, M. D. Heinemann, C. A. Kaufmann, J. L. Garcia, V. Izquierdo, X. Fontané, T. Goislard, M. C. Lux-Steiner, and S. Gledhill, "An overview of technological aspects of Cu(In,Ga)Se_2 solar cell architectures incorporating ZnO nanorod arrays," *physica status solidi (a)*, vol. 212, no. 1, pp. 76–87, 2015.

[22] C. van Lare, G. Yin, A. Polman, and M. Schmid, "Light coupling and trapping in ultrathin Cu(In,Ga)Se_2 solar cells using dielectric scattering patterns," *ACS Nano*, vol. 9, no. 10, pp. 9603–9613, 2015.

[23] I. Massiot, N. Vandamme, N. Bardou, C. Dupuis, A. Lemaître, J.-F. Guillemoles, and S. Collin, "Metal nanogrid for broadband multiresonant light-harvesting in ultrathin GaAs layers," *ACS Photonics*, vol. 1, no. 9, pp. 878–884, 2014.

[24] S. Collin, N. Vandamme, J. Goffard, A. Cattoni, A. Lemaitre, and J. F. Guillemoles, "Ultrathin GaAs solar cells with a nanostructured back mirror," in *Photovoltaic Specialist Conference (PVSC), 2015 IEEE 42nd*, 2015, pp. 1–3.

[25] V. E. Ferry, M. A. Verschuuren, H. B. T. Li, E. Verhagen, R. J. Walters, R. E. I. Schropp, H. A. Atwater, and A. Polman, "Light trapping in ultrathin plasmonic solar cells," *Optics Express*, vol. 18, p. A237, 2010.

[26] V. E. Ferry, M. A. Verschuuren, M. C. v. Lare, R. E. I. Schropp, H. A. Atwater, and A. Polman, "Optimized spatial correlations for broadband light trapping nanopatterns in high efficiency ultrathin film a-Si:H solar cells," *Nano Letters*, vol. 11, no. 10, pp. 4239–4245, 2011.

[27] P. Lalanne and G. M. Morris, "Highly improved convergence of the coupled-wave method for TM polarization," *Journal of the Optical Society of America A*, vol. 13, no. 4, p. 779, 1996.

[28] L. Li, "New formulation of the fourier modal method for crossed surface-relief gratings," *Journal of the Optical Society of America A*, vol. 14, no. 10, p. 2758, 1997.

[29] P. Lalanne and M. P. Jurek, "Computation of the near-field pattern with the coupled-wave method for transverse magnetic polarization," *Journal of Modern Optics*, vol. 45, no. 7, pp. 1357–1374, 1998.
[30] P. Lalanne and J. P. Hugonin, "Reticolo software for grating analysis." [Online]. Available: https://www.lp2n.institutoptique.fr/Membres-Services/Responsables-d-equipe/LALANNE-Philippe
[31] P. Paulson, R. Birkmire, and W. Shafarman, "Optical characterization of $CuIn_{1-x}Ga_xSe_2$ alloy thin films by spectroscopic ellipsometry," *Journal of Applied Physics*, vol. 94, no. 2, pp. 879–888, 2003.
[32] T. Hara, T. Maekawa, S. Minoura, Y. Sago, S. Niki, and H. Fujiwara, "Quantitative assessment of optical gain and loss in submicron-textured $CuIn_{1-x}Ga_xSe_2$ solar cells fabricated by three-stage coevaporation," *Phys. Rev. Applied*, vol. 2, p. 034012, Sep 2014.
[33] S. Minoura, T. Maekawa, K. Kodera, A. Nakane, S. Niki, and H. Fujiwara, "Optical constants of Cu(In, Ga)Se_2 for arbitrary cu and ga compositions," *Journal of Applied Physics*, vol. 117, no. 19, p. 195703, 2015.
[34] A. Loubat, C. Eypert, F. Mollica, M. Bouttemy, N. Naghavi, D. Lincot, and A. Etcheberry, "Optical properties of ultrathin {CIGS} films studied by spectroscopic ellipsometry assisted by chemical engineering," *Applied Surface Science*, p. available online, 2016.
[35] N. Ehrmann and R. Reineke-Koch, "Ellipsometric studies on ZnO:Al thin films: Refinement of dispersion theories," *Thin Solid Films*, vol. 519, no. 4, pp. 1475–1485, 2010.
[36] E. D. Palik, *Handbook of Optical Constants of Solids*. Academic Press, 2012.
[37] P. B. Johnson and R. W. Christy, "Optical constants of the noble metals," *Physical Review B*, vol. 6, no. 12, pp. 4370–4379, 1972.

ACKNOWLEDGMENT

The authors gratefully acknowledge Jérôme Michallon for fruitful discussions. This work was partly supported by the French ANR project ULTRACIS-M (ANR-12-PRGE-0003), and by the H2020-NMBP European project ARCIGS-M.

APPENDIX A
REFRACTIVE INDICES

The refractive indices used in this article are plotted in Figure 7. The optical properties of CIGS films are strongly dependent of the elemental compositions, and comparison between experiments and simulations can be hindered by heterogeneities and composition gradients. Here we have taken CIGS optical data from reference [31] with a correction close to the gap to avoid residual absorption for photon energies below the bandgap. It results in numerical results consistent with experiments (see Appendix B). Alternative optical data can be found in references [32]–[34].

APPENDIX B
COMPARISON WITH PUBLISHED EXPERIMENTS

Figure 8(a) shows the CIGS absorption spectra calculated for two different CIGS thicknesses and various stacks for the back contact. These numerical results are compared to external quantum efficiency measurements (b) taken from reference [10]. In the 300-900 nm wavelength range, a quantitative agreement is found for most structures ($1.8\ \mu$m and $0.4\ \mu$m with Al_2O_3/MgF_2 and 50 nm of Al_2O_3). The main discrepancies are attributed to the differences in the refractive indices: the simulated structures exhibit less parasitic absorption in the CdS or ZnO:Al layers ($\lambda \simeq 500$ nm), and less CIGS absorption in the long wavelength range ($\lambda > 900$ nm) due to a smaller bandgap. The resulting Jsc are comparable. The numerical results further confirm that the low EQE measured with no passivation layers (blue curve in Figure 8(a)) is due to a poor collection efficiency of charge carriers.

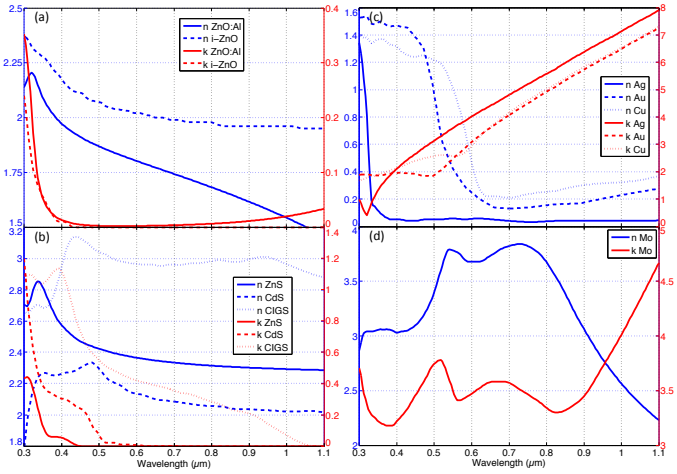

Figure 7. (a) Refractive index of ZnO:Al [35] and i-ZnO, from ellipsometry measurements. (b) Refractive index of ZnS and CdS from reference [36] and of CIGS from reference [31]. (c) Refractive index of Ag, Au and Cu, from reference [37]. (d) Refractive index of Mo from reference [36].

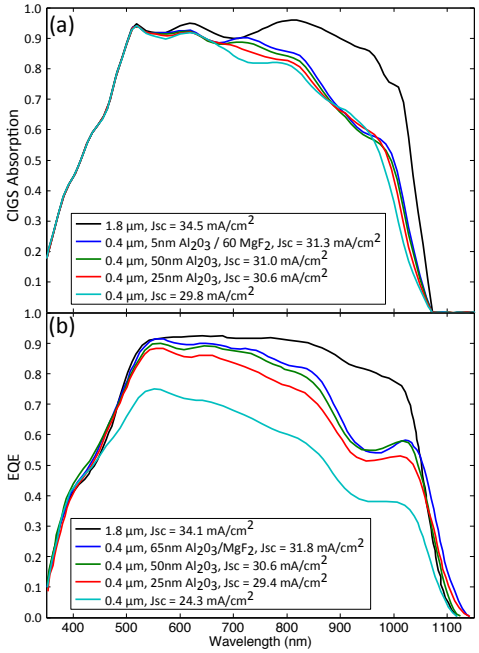

Figure 8. Calculated absorption (a) and measured external quantum efficiency (EQE) of planar CIGS solar cells with different thicknesses and back contacts. Experimental data of (b) are taken from reference [10].

APPENDIX C
NUMERICAL RESULTS FOR VARIOUS COMBINATIONS OF BUFFER LAYERS, THICKNESSES AND BACK MIRRORS

Table I
NUMERICAL RESULTS OBTAINED FOR JSC WITH DIFFERENT BUFFER LAYERS, CIGS THICKNESSES AND FLAT BACK MIRRORS.

Buffer layer	CIGS thickness (nm)	Jsc (mA/cm^2) (Flat mirror)			
		Mo	Cu	Au	Ag
CdS	100	18.3	22.0	23.4	24.3
	150	22.4	26.7	28.0	28.4
	200	25.7	30.0	31.0	31.4
	250	27.0	30.1	31.4	31.6
	300	28.3	31.0	32.3	32.5
	350	29.7	32.2	33.5	33.7
	400	30.5	32.7	33.8	34.0
	450	31.0	32.7	33.9	34.0
	500	31.6	33.0	34.4	34.5
ZnS	100	18.8	25.4	25.8	26.8
	150	23.5	29.7	30.1	30.7
	200	26.5	32.4	32.7	33.2
	250	28.6	33.2	33.4	33.8
	300	30.4	34.4	34.6	34.8
	350	31.7	35.5	35.6	35.8
	400	32.6	35.7	35.8	36.0
	450	33.5	36.0	36.1	36.3
	500	34.1	36.6	36.7	36.8

Table II
NUMERICAL RESULTS OBTAINED FOR JSC WITH DIFFERENT BUFFER LAYERS, CIGS THICKNESSES AND NANOSTRUCTURED BACK MIRRORS FOR STRUCTURES A (NANOGRID OF HEIGHT: 100 NM, WIDTH: 100 NM, PERIOD: 300 NM) AND B (PILLARS OF HEIGHT: 175 NM, WIDTH: 325 NM, PERIOD: 575 NM).

Buffer layer	CIGS thickness (nm)	Jsc (mA/cm^2) (Nanostructured mirror)		
		Cu	Au	Ag
CdS with structure A	100	26.5	27.4	31.2
	150	30.2	31.1	34.1
	200	31.7	32.4	34.7
	250	32.2	32.8	34.7
	300	33.2	33.8	35.3
	350	33.8	34.3	35.6
	400	33.9	34.3	35.4
	450	34.3	34.6	35.6
	500	34.7	35.0	36.0
CdS with structure B	100	25.8	26.8	29.5
	150	29.9	30.1	33.0
	200	32.0	32.7	34.4
	250	32.7	33.2	34.6
	300	33.6	34.0	35.3
	350	34.1	34.5	35.4
	400	34.7	35.1	35.9
	450	34.7	35.0	35.6
	500	35.1	35.3	35.9
ZnS with structure A	100	28.8	29.8	33.8
	150	32.3	33.1	36.2
	200	33.6	34.4	36.7
	250	34.5	35.1	37.0
	300	35.5	36.0	37.6
	350	35.9	36.4	37.7
	400	36.1	36.5	37.6
	450	36.5	36.9	38.0
	500	36.8	37.2	38.1
ZnS with structure B	100	27.9	29.0	31.8
	150	32.2	33.1	35.4
	200	33.9	34.6	36.3
	250	34.9	35.5	36.9
	300	35.6	36.1	36.9
	350	36.6	37.0	38.0
	400	36.7	37.1	38.0
	450	36.9	37.2	38.0
	500	37.2	37.5	38.1